Heliyon 9 (2023) e19055

Contents lists available at ScienceDirect

Heliyon

journal homepage: www.cell.com/heliyon

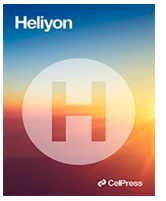

High-temperature tribological performance of stir-cast and heat-treated EV31A magnesium alloy: Experiments and predictions

M. Somasundaram [a], U. NarendraKumar [a,**], A. Raja Annamalai [b,*], A. Muthuchamy [c]

[a] Department of Manufacturing Engineering, School of Mechanical Engineering, Vellore Institute of Technology, Vellore, 632 014, Tamilnadu, India
[b] Centre for Innovative Manufacturing Research, Vellore Institute of Technology, Vellore, 632 014, Tamil Nadu, India
[c] Department of Metallurgical and Materials Engineering, National Institute of Technology, Tiruchirappalli, Tamil Nadu, 620 015, India

ARTICLE INFO

Keywords:
Magnesium alloy
Rare earth elements
High-temperature wear
Dry sliding wear
Tribological properties
Machine learning

ABSTRACT

The temperature effect on the wear behaviour of EV31A Mg alloy during dry sliding wear was investigated. Wear tests were carried out at 50, 100, 150, 200, and 250 °C using a standard load of 10 N and a sliding distance of 1000 m. Weight loss method was used to calculate the wear rate. Optical microscopy was used to examine the microstructure of the EV31A alloy. FE-SEM with EDS analysis was used to investigate the wear morphology, and XRD analysis was performed both before and after the wear test. A high wear coefficient (K) value (more than 10^{-4}) indicates extreme wear for EV31A in all the scenarios. T4 EV31A had a maximum wear rate of 20.2 mg at 150 °C. The as-cast EV31A alloy exhibits an excellent wear rate at the price of mechanical properties under all test scenarios. Wear resistance is improved by Nd and Zr oxides, although Mg and Gd oxides have little effect. Zn has no effect on the wear behaviour of the EV31A. In as-cast, T4, and T6 heat-treated conditions, the EV31A alloy exhibits delamination (abrasive wear), oxide development (corrosive wear), and delamination mixed with plastic deformation (adhesive wear). A Three-layered ANN and adapted Fine Gaussian SVM predicted tribological characteristics. In ANN prediction, the maximum R^2 was 0.99 for CoF and 0.89 for wear rate, respectively. Despite the fact that the study's normal load is constant, machine learning models allow to deduce that temperature and normal load are the main influential parameters in CoF and wear rate, respectively.

1. Introduction

Over the course of several decades, great strides have been made to decrease the weight and heat production in the electronic industry [1], as well as to increase fuel efficiency in the automotive, aerospace, and aviation sectors [2,3]. Lightweight metals like aluminum (Al), titanium (Ti), and magnesium are in high demand as a result (Mg). Although Mg is lightweight, it is very difficult to process because of its high affinity towards oxygen, leading to severe oxidation and burning of materials at high temperatures. The difficulty in processing Mg-based alloys hinders the usage of Mg [4–6]. The processing of Mg in an inert gas atmosphere is a better

* Corresponding author.
** Corresponding author.
E-mail addresses: u.narendrakumar@vit.ac.in (U. NarendraKumar), raja.annamalai@vit.ac.in (A.R. Annamalai), Muthuchamy@nitt.edu (A. Muthuchamy).

https://doi.org/10.1016/j.heliyon.2023.e19055
Received 17 March 2023; Received in revised form 7 August 2023; Accepted 9 August 2023
Available online 12 August 2023

Table 1
Details of heat-treatment processes [34].

Heat Treatment Process	T4 Condition		T6 Condition	
	Temperature (°C)	Time (Hours)	Temperature (°C)	Time (Hours)
Solid Solutionizing	520	8	520	8
Water Quenching	60 to 80	1 min	60 to 80	1 min
Age-hardening	–	–	200	16

choice to overcome the processing difficulty. The Mg and its alloys are processed in the solid and liquid states. The solid-state processing involves compaction and sintering of Mg with its alloying elements, followed by secondary processes such as rolling and extrusion [7,8]. The liquid processing of Mg involves various types of casting processes. Among the various casting methods, stir casting is considered an economical and high-yield method to prepare Mg-based components [9]. Especially while adding heavy alloying elements to the Mg, the stir casting process dramatically helps to avoid segregation or agglomeration of alloying elements. Due to its low density and outstanding strength-to-weight ratio, Mg has been singled out as the future material of choice among numerous lightweight materials [10–13]. In the railway industry, friction and wear rate are extremely important factors in determining a material's effectiveness, especially in rolling stocks. The demand for high-speed rail is rising in many parts of the world, posing a problem for the industry's long-term viability [14,15]. Lightweight materials are used in railway body parts to reduce energy-induced impact during collisions [16,17] and to decrease friction and wear between the rail and wheel contact. Because it is lightweight and has the requisite mechanical qualities, magnesium is being evaluated for use in the railway industry. Theoretically, Mg could cause a weight loss of 8.6%–12.6%, according to certain sources [13]. Furthermore, Mg and its alloys are subjected to different automobile parts, where the parts undergoes repeated sliding motion which creates heat. Therefore, it is important to learn about the tribological characteristics of Mg alloys. However, Mg's weak ductility, formability, and limited slip activation [18] stem from its hexagonal close-packed (HCP) structure, limiting its potential uses. There have been several attempts to boost the mechanical characteristics and manufacturing viability of Mg alloys, however, these areas still have room to grow [19,20]. The report says many Mg and its alloys have undergone dry sliding wear tests by varying the parameters such as sliding velocity and normal load. The studies also reported the influence of these parameters on wear rate, CoF, and wear mechanism [21,22].

Importantly, the operating temperature determines whether moderate wear progresses to severe wear, however, the effect of temperature on Mg's tribological characteristics is not addressed in depth. According to the findings, a change from mild to severe wear occurs when the bulk surface temperature rises to just above the critical point [23]. High-temperature wear behaviour of Mg–Al-based alloys is investigated in the literature [24–26]. Yet research on the wear behaviour of REE-based Mg alloys at elevated temperatures is lacking. There has not been sufficient systematic research on the features and processes of wear at high temperatures [27]. In the early 20th century, machine learning was explored in various fields of research, including medicine, engineering, computer vision, etc. Machine learning helps predict or forecast data based on predefined data without any explicit programme [28]. So machine learning methods can be well-suitable to predict complicated data through experimentation. Quantitative experimentation to analyze the wear rate of the materials is also tricky because of its dependence on mechanics, physics, chemistry, and materials science [26,29]. Recently, an attempt has been made to predict the wear behaviour of ZK60/CeO_2 composites with the limited dataset and compared with the experimental data. It helped in the development of a superior model [30]. The study on the prediction of the wear behaviour of AZ31 Mg alloy shows that the wear rate is proportional to load and inverse relation to sliding speed. It also confirms XGBoost Machine learning (ML) model shows a good correlation between training and testing data with R^2 of 0.999 and 0.908, respectively [31].

Previous studies show that the REE-based intermetallic phases such as $Mg_{12}Nd$, $Mg_{41}Nd_5$, REE-Zn, etc., were significantly influence the electrochemical behaviour of the EV31A Mg alloy. The corrosion rate of the alloy is restricted by intermetallic phases and localized galvanic corrosion is reported [32]. The oxidation rate of the EV31A increases with an increase in temperature, due to the change in activation energy [33]. Further heat treatment of REE-based Mg alloys improves mechanical (hardness, tensile properties) and oxidation qualities at the expense of ductility due to the better mechanical properties of these alloys [33,34]. Since this is the case, investigating their wear patterns is equally crucial, as heat treatment and working temperature are influencing the behaviour of the EV31A alloy. The purpose of this study is to compare the wear behaviour of as-cast, T4, and T6 heat-treated REE-Mg alloys while working at extreme temperatures (EV31A). Because of its dependence on mechanics, physics, chemistry, and materials science, quantitatively predicting wear rate is also difficult. However, based on already published research works, an attempt was made to forecast the wear rate and CoF of EV31A using machine learning approaches and the prediction was then compared to experimental results.

2. Experimentation details

2.1. Specimen preparation

The alloy of the study was prepared by the stir-casting process by melting the Mg at 650 °C and adding the alloying elements of the required weight percentage (Nd = 2.5–3.5%; Gd = 0.5–1.5%; Zn = 0.2–0.5%; Zr = 0.2–0.5%). Further details of material preparation are given in the previous work [34]. Table 1 details the parameters of the T4 and T6 heat treatment processes applied to the stir-cast EV31A alloy. Stir-cast, T4, and T6 heat-treated EV31A were subjected to a dry sliding wear test. The pin (specimen) was made with a

diameter of 8 mm and a height of 30 mm; it was then polished on one side using emery papers of varying grits, and finally in velvet fabric lubricated with alumina slurry.

2.2. Tribological test

The pin's polished surface was rubbed against the disc 535A99 steel (EN31's equivalent) in a high-temperature tribological tester to simulate wear. To get an accurate reading of the temperature of the specimen in real-time was measured by embedded thermocouple within the specimen. The dry sliding wear test was conducted at 50 °C, 100 °C, 150 °C, 200 °C, and 250 °C with a normal load of 10 N, a sliding speed of 1 m/s, and a sliding distance of 1000 m. Fifteen samples were analyzed, with five in each of three different circumstances (as-cast; T4; T6). The testing results include the friction coefficient (CoF) and the wear rate in terms of weight loss (mg). In order to understand the wear behaviour of the EV31A, the experimentation and measurement of wear rate and CoF were performed based on ASTM G99 – 17. The tribological testing was carried out only to understand general wear behaviour of EV31A at elevated temperature and effect of heat treatment on it.

2.3. Characterization

Optical microscopy was used to examine the alloy's microstructure (Carl Zeiss and Axio Lab Al). To compare the hardness of the specimen before and after the wear test, a Vickers hardness tester was used with a load of 50 gm and a dwell period of 15s. X-Ray Diffraction (XRD) (Bruker, D8-Advance P-XRD) with CuKα (1.5406) radiation at a scanning range of 20°–90° was used to evaluate the presence of distinct phases before and after wear. Field emission-scanning electron microscopy (FE-SEM) (Thermo Fisher Scientific FEI Quanta 250 FEG) with energy-dispersive X-ray spectroscopy (Oxford) was used to detect wear morphology and element distribution on the worn surface (FE-SEM with EDS).

2.4. Machine learning methodology

The machine learning (ML) methodology was adapted to predict the coefficient of friction (CoF) and wear rate. The dataset for the study was collected from various literature by considering operating temperature (ºC), hardness of the workpiece and counterpart (HV), normal load (N), the weight percentage of Mg and REE (%) as input parameters and CoF and wear (mm^3/Nm) as response variables [35–44]. For the purpose of comparison, the experimental wear rate in mg is converted into mm^3/Nm. Two different ML methods, viz support vector machines (SVM) and artificial neural network (ANN) are utilized to predict the tribological properties of the EV31A Mg alloy. Both SVM and ANN model can solve regression and classification problems with greater complexity differently.

2.4.1. Support vector machines (SVM)

The SVM is utilized primarily for data with an irregular distribution since the kernel function of the model aids in generalization by converting the input data to high dimensional data, hence preventing overfitting. Furthermore, the model's hyperplane aids in data classification, and convex optimization aids in achieving the global minimum error rather than the local least error. SVM takes less time to compute than ANN and other machining learning models. Because of its high flexibility and ability to rapidly vary the response function, the fine Gaussian model is chosen among several SVM regression models for the prediction of tribological parameters. In this work, the fine Gaussian SVM model with kernel scale of 0.61, Box constraint of 0.1909, and Epsilon of 0.01909 is utilized. The mathematical expression of the Gaussian function and expression to predict the response using the SVM model are shown in Eqn. 1, and 2, respectively.

$$G(x_j, x_k) = exp\left(\left\|x_j - x_k\right\|^2\right) \tag{1}$$

$$f(x) = \sum_{n=1}^{N} (\alpha_n - \alpha_n^*) G(x_n, x) + b \tag{2}$$

"The property α of a trained SVM model stores the difference between two Lagrange multipliers of support vectors, ($\alpha_n - \alpha_n^*$). The properties Support Vectors and Bias store x_n and b, respectively" [45–47].

2.4.2. Artificial neural network (ANN)

The communication of biological neurons in the human cerebrum inspired the Artificial Neutral Network (ANN). The ANN model attempts to link many input variables to their corresponding output variables by translating data across different neurons while taking note of current data and attempting to create a probable relationship between them. This approach can mine massive volumes of data, even in extremely intricate scenarios. Notably, because the ANN model imposes no limits or boundaries on the input data, it is appropriate for non-linear data having complicated relationships with its response. In this study, a three-layered artificial neural network (ANN) with a hidden layer of (10, 10, 10) and an activation function of ReLU is used. The ANN model is made up of three parts, which are as follows: (i) input layer - nodes provide input to the hidden layer; no processing occurs. (ii) Hidden layers - provide weightage based on the activation function, which is a component of the hidden layers; (iii) output layer - provides output based on processed data. Eqns. (3)–(4) gives the mathematical representation of the ANN model:

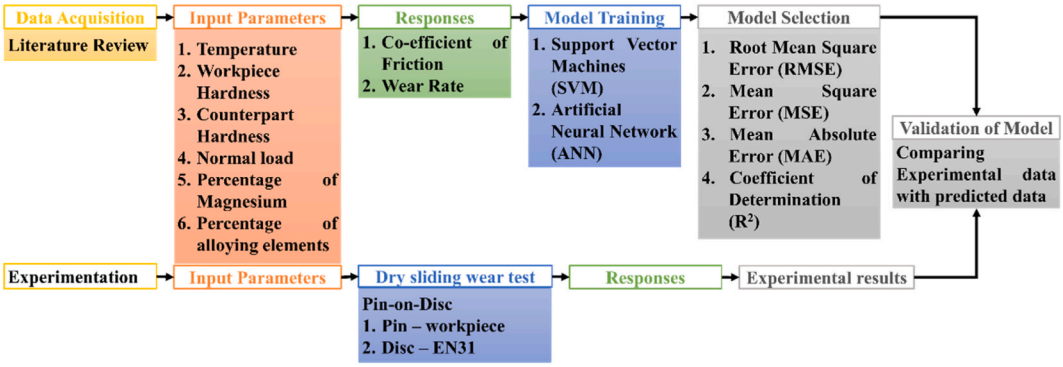

Fig. 1. Methodology of the study on tribological properties of EV31A.

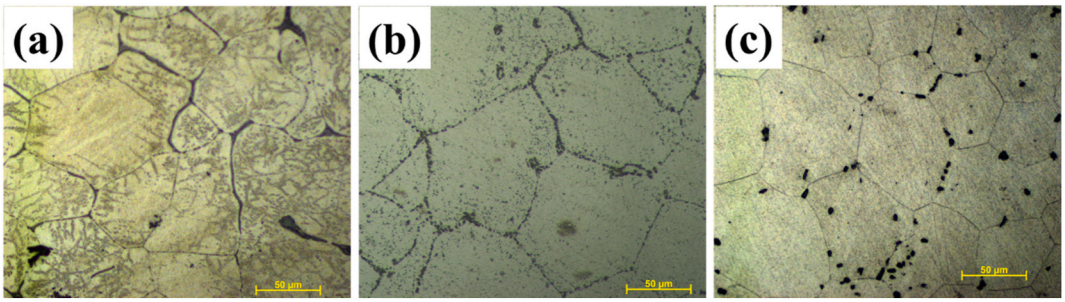

Fig. 2. Optical Microscopy of EV31A (a) as-cast; (b) T4; (c) T6 heat-treated conditions.

$$I_j = \sum_{i=1}^{n} \left(w_{ij} x_i + b_j \right) \tag{3}$$

$$O_j = \psi \left(I_j \right) \tag{4}$$

"where x_i denotes the inputs, w_{ij} the connection weight, b_j the bias, I_j the hidden layer neuron's input, Ψ the activation function, and O_j the hidden layer neuron's output" [47].

2.4.3. Performance metrics

The defined models were validated by a cross-fold validation method with 10-folds. The result is reported with performance metrics such as coefficient of determination (R^2) measures the proportion of variance in the output variable, the root mean square error (RMSE) establishes the average distance between predicted and actual values, the mean square error (MSE) is the square of RMSE and amplifies larger errors, and the mean absolute error (MAE) estimates the absolute error between predicted and actual values. In the case of RMSE, the smallest value is favoured. The RMSE includes the MAE as well as additional information on the error variance (biased estimator). The increased sensitivity of RMSE to a small number of outliers is directly due to absolute error variation [48]. The F-test evaluates the effect of process variables on response. It is the statistical test that follows an F-distribution under the null hypothesis [49]. Finally, the predicted results are compared with experimental results, as shown in Fig. 1. Each model is trained twice with the same process parameters and with different responses (CoF and wear rate). eqns. (5)–(8) shows the formula to calculate the performance metrics such as MAE, MSE, RMSE, and R^2, respectively.

$$MAE = \frac{1}{N} \sum_{i=1}^{N} |y_i - \hat{y}| \tag{5}$$

$$MSE = \frac{1}{N} \sum_{i=1}^{N} (y_i - \hat{y})^2 \tag{6}$$

$$RMSE = \sqrt{\frac{1}{N} \sum_{i=1}^{N} (y_i - \hat{y})^2} \tag{7}$$

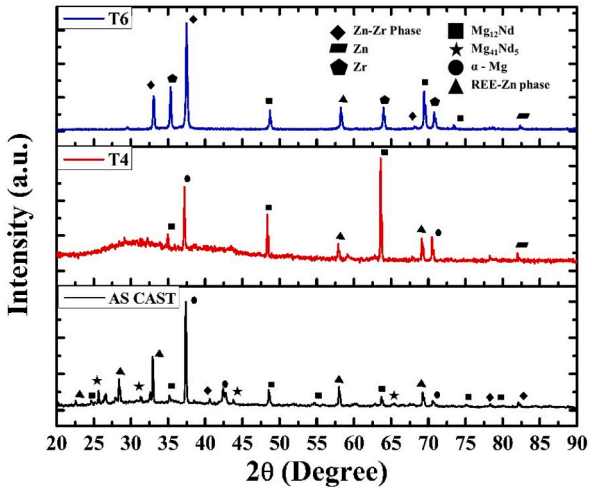

Fig. 3. XRD analysis of EV31A test specimen before wear test [34].

$$R^2 = 1 - \frac{\sum (y_i - \hat{y})^2}{\sum (y_i - \bar{y})^2} \tag{8}$$

where N is the number of data points; $\hat{y}$ is the predicted output; y is the actual output; $\bar{y}$ is the mean of all output parameters.

3. Results and discussions

3.1. Microstructural analysis

Fig. 2 (a – c) shows the optical microscopy of EV31A alloy, which is used to measure the grain size using the linear intercept method. The average grain size of the as-cast, T4, and T6 heat-treated EV31A alloy is 43.67 ± 3.31 μm, 67.51 ± 1.82 μm, and 37.16 ± 2.02 μm, respectively. Also, the average number of grains per square inch at a magnification of 100× was reported as 32, 8, and 32 in as-cast, T4, and T6 heat-treated conditions, respectively [50,51]. In as-cast alloy, intermetallic phases tend to segregate at the grain boundary, as seen in Fig. 2(a). As can be seen in Fig. 2(b), the precipitated intermetallic phases are dissolved during the T4 heat treatment process, and the T6 heat treatment procedure refines the grains. As confirmed by XRD analysis and EDS mapping in our earlier study [34], the dark patches on grain boundaries in Fig. 2(c) are the Zn–Zr phase.

Fig. 3 shows the presence of the phase in EV31A before the wear test. The as-cast alloy is dominated by intermetallic phases such as $Mg_{41}Nd_5$, $Mg_{12}Nd$, and Gd–Zn. T4 heat treatment resulted in the dissolution of the unstable intermetallic phase $Mg_{41}Nd_5$ and Zn_2Zr_3. The reduction of the other intermetallic phases leads to the domination of α-Mg peaks. The tetragonal structure of $Mg_{12}Nd$ creates a challenge in the dissolution of the phase during the T4 heat treatment process. Also, the solubility limit of Nd in Mg at 520 °C is 1.87 wt %, which limits the dissolution of Mg–Nd intermetallics [52]. The solubility limit of Gd in Mg at 548 °C is 23.49 wt%, resulting in the dissolution of the Gd–Zn intermetallic phase during the T4 heat treatment process, and the solubility limit decreases exponentially. Its solubility at 200 °C is 3.82 wt%. Therefore, a Gd-based Mg alloy is ideal for age-hardening [53,54]. Furthermore, the solubility limit of the Zr phase in Mg depends on the percentage of Zn, where the Zn act as a grain-refiner in the EV31A alloy system where [55,56]. So, the Zn–Zr phase, Zn, Zr, are formed by T6 heat treatment.

3.2. Co-efficient of friction and wear rates

The relative density of the prepared EV31A Mg alloy is determined based on the Archimedes principle, which is 97.4%, and it is also reported in our previous study [34]. The relative density has been measured in the sample size of 10 mm × 10 mm x 5 mm, taken from the prepared cast block's top, middle, and bottom surfaces of 245 × 215 × 30 mm. This decrease in relative density is primarily due to the formation of zero-dimensional defects such as gas, and shrinkage pores, and other casting defects such as one-dimensional (cold-shut, misruns, cracks), two-dimensional (pinholes, sand wash, and rat tails), and three-dimensional (shrinkage, warpage) defects, during the stir-casting process, which reduces the density by 2.6%. The porosity of 4% is acceptable in cast products, as per standards [57,58]. It is confirmed that the prepared alloy is an acceptable cast product. Also, the study primarily focuses on analyzing the effect of heat treatment and temperature on the wear behaviour of EV31A.

The EV31 alloy has a Vickers microhardness of 83 $HV_{0.05}$ in the stir-cast condition, 91 $HV_{0.05}$ in the T4 heat-treated condition, and 98 $HV_{0.05}$ in the T6 heat-treated condition. The hardness of the alloy increases during the heat treatment process, regardless of grain size [34]. The rise in hardness in T4 EV31A correlates to the dissolution of intermetallic phases, and following the T6 heat treatment process, the meta-stable intermetallic ($Mg_{12}Nd$) dissolved and the creation of a Zn–Zr precipitate. Microhardness is increased due to an

Table 2
Experimental results of high temperature dry sliding tribological test

Temp.	Hardness ($HV_{0.05}$)			CoF			Wear rate (mg)			Wear Co-efficient		
	As-cast	T4	T6	As-cast	T4	T6	As-cast	T4	T6	As-cast	T4	T6
50 °C	94.4 ± 5.1	120.8 ± 5.8	120.1 ± 7.0	0.47	0.39	0.45	14.6	15.1	19.3	0.0792	0.1047	0.1332
100 °C	102.8 ± 6.9	108.4 ± 3.8	126.7 ± 1.8	0.53	0.25	0.44	14.2	17.7	17.2	0.0838	0.1105	0.1252
150 °C	90.2 ± 2.2	115.1 ± 2.2	131.1 ± 3.2	0.56	0.17	0.25	14.5	20.2	14.7	0.0751	0.1334	0.1107
200 °C	87.1 ± 6.5	115.4 ± 4.4	132.4 ± 3.3	0.36	0.07	0.29	16.4	13.8	18.1	0.0820	0.0915	0.1376
250 °C	85.0 ± 2.8	100.6 ± 4.8	122.0 ± 3.2	0.30	0.06	0.47	17.0	07.3	18.4	0.0830	0.0422	0.1293

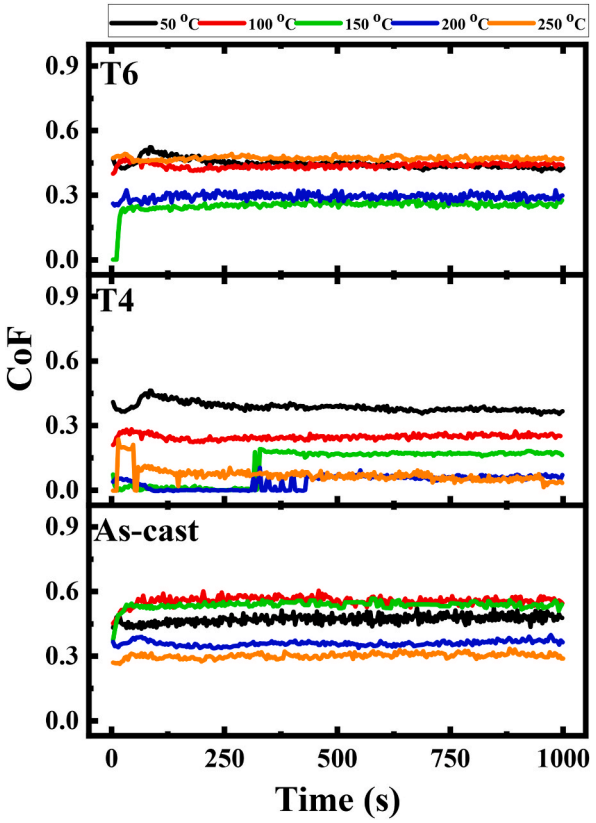

Fig. 4. Coefficient of friction as-cast, T4, and T6 EV31A.

increase in homogeneity and redistribution of secondary intermetallic phases [59]. A dry sliding wear test at a high temperature was performed, and the microhardness of the test specimen after the wear test was measured; the findings are presented in Table 2. Because the microstructure and phases in the test specimens influence the alloy's hardness, a correlation between hardness and the wear rate of the EV31A is established.

Fig. 4 shows the CoF as a function of sliding time with the wear temperature of 50 °C, 100 °C, 150 °C, 200 °C, and 250 °C of as-cast, T4, and T6 heat-treated EV31A respectively. The impact of temperature on mean CoF can be more easily grasped with the data represented in Table 2. In all cases except wear of the T6 heat-treated alloy, the as-cast had a greater CoF than the heat-treated alloy at 250 °C. The highest CoF of 0.56 is recorded in as-cast alloy at 150 °C. The lowest CoF of 0.06 is recorded in T4 heat-treated alloy at 250 °C. As a rule, as-cast EV31A has a lower CoF than T6 or T4 heat-treated EV31A. The as-cast alloy has a higher CoF below 100 °C and a lower CoF above 100 °C. The coefficient of friction (CoF) declines with increasing temperature in heat-treated alloy T4 but remains practically unchanged in T6 up to temperatures of 50 °C and 100 °C, it decreases with 150 °C, and again it starts to increase with temperature. T4 alloy has a lower CoF than as-cast and T6 EV31A due to the grain size of the alloy. The greater grain size indicates a lower grain boundary density, which reduces dislocation activity and facilitates deformation via grain boundary sliding or other lower CoF methods. Furthermore, as the working temperature rises above 200 °C, the CoF of T4 EV31A falls drastically below 0.07. It is due to the presence of a meta-stable $Mg_{12}Nd$ intermetallic phase, which transforms the alloy from a brittle hexagonal close-packed (HCP) structure to a body centred cubic (BCC) structure, enhancing ductility and lowering the CoF.

Wear is defined as the 'progressive loss of substance from the operating surface of a body occurring as a result of relative motion at

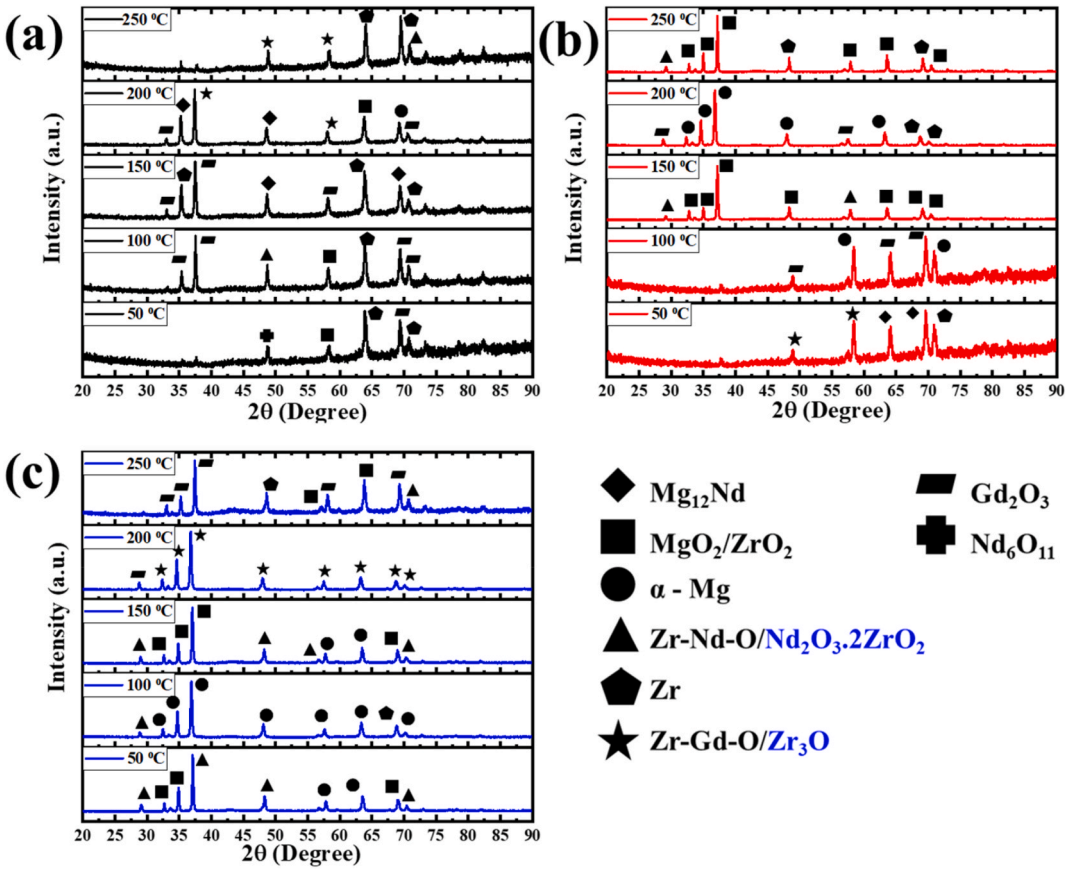

Fig. 5. XRD results of EV31A after wear test; (a) As-cast; (b) T4; (c) T6 heat treated alloy.

the surface [60]. However, this is not a physical attribute but rather an inherent response of the system. The wear rate of EV31A was displayed in Table 2 under various test settings. The wear rate of the as-cast EV31A alloy is consistent across all temperatures. In contrast, wear rates for T4 and T6 heat-treated alloys increase and decrease, respectively, until 150 °C and then start to decrease to 7.3 mg and increase up to 18.4 mg at 250 °C, respectively. The maximum and minimum wear rate of 20.2 and 7.3 mg is recorded in wear temperature of 150 °C and 250 °C, respectively, in T4 heat-treated EV31A. The as-cast and T6 alloy show the minimum wear rate of 14.2 mg and 14.7 mg at 100 °C and 150 °C, respectively and the maximum wear rate recorded at 250 °C and 50 °C, respectively is 17 mg and 19.3 mg. The as-cast and T6 alloy show a similar trend of CoF and wear rate in different testing temperature.

Eqn. (9) gives the relation between wear rate and hardness, which is known as the Archard wear equation [61].

$$Q = \frac{KW}{H} \tag{9}$$

"Where Q is the volume removed from the surface per unit sliding distance, W is the normal load applied to the surface by its counter body, and H is the indentation hardness of the wearing surface. Therefore, K is a dimensionless quantity called the wear coefficient". The severity of the wear process can be measured with the aid of this dimensionless parameter. Wear due to dry sliding is said to have a K value between 10^{-2} – 10^{-6}. If K is from 10^{-2} to $10^{-4,}$ it is called severe wear; if K is less than 10^{-4}, it is referred to as mild wear [62]. Severe wear behaviour is characterized by substantial material transfer to the counter face and widespread surface damage, whereas mild wear behaviour is characterized by relatively little surface damage and a tribological layer covering the surface. Table 2 clearly shows that all test conditions K value is greater than 10^{-4}, which implies EV31A undergoes severe wear in all test cases. Although T4 heat-treated alloy shows the lowest K of 0.0422, typically, it is also noteworthy to notice that the K value of as-cast EV31A is less than heat-treated alloy. Eq. (1) is true in all test conditions, which clearly shows that the hardness of the specimen is inversely proportional to the wear volume removed per unit sliding distance.

3.3. XRD analysis before and after wear

Fig. 5(a–c) shows the phases in the as-cast, T4, and T6 heat-treated EV31A alloy after the wear test. In as-cast alloy, the oxides of Mg, Zr, and Zr–Nd are observed in the wear temperature of 50 °C, 100 °C, and 150 °C. On the other hand, the oxides of Gd, Zr, and Gd–Zr are detected at the wear temperature of 200 °C and 250 °C, but it does not resist the wear rate of the EV31A, as a maximum wear

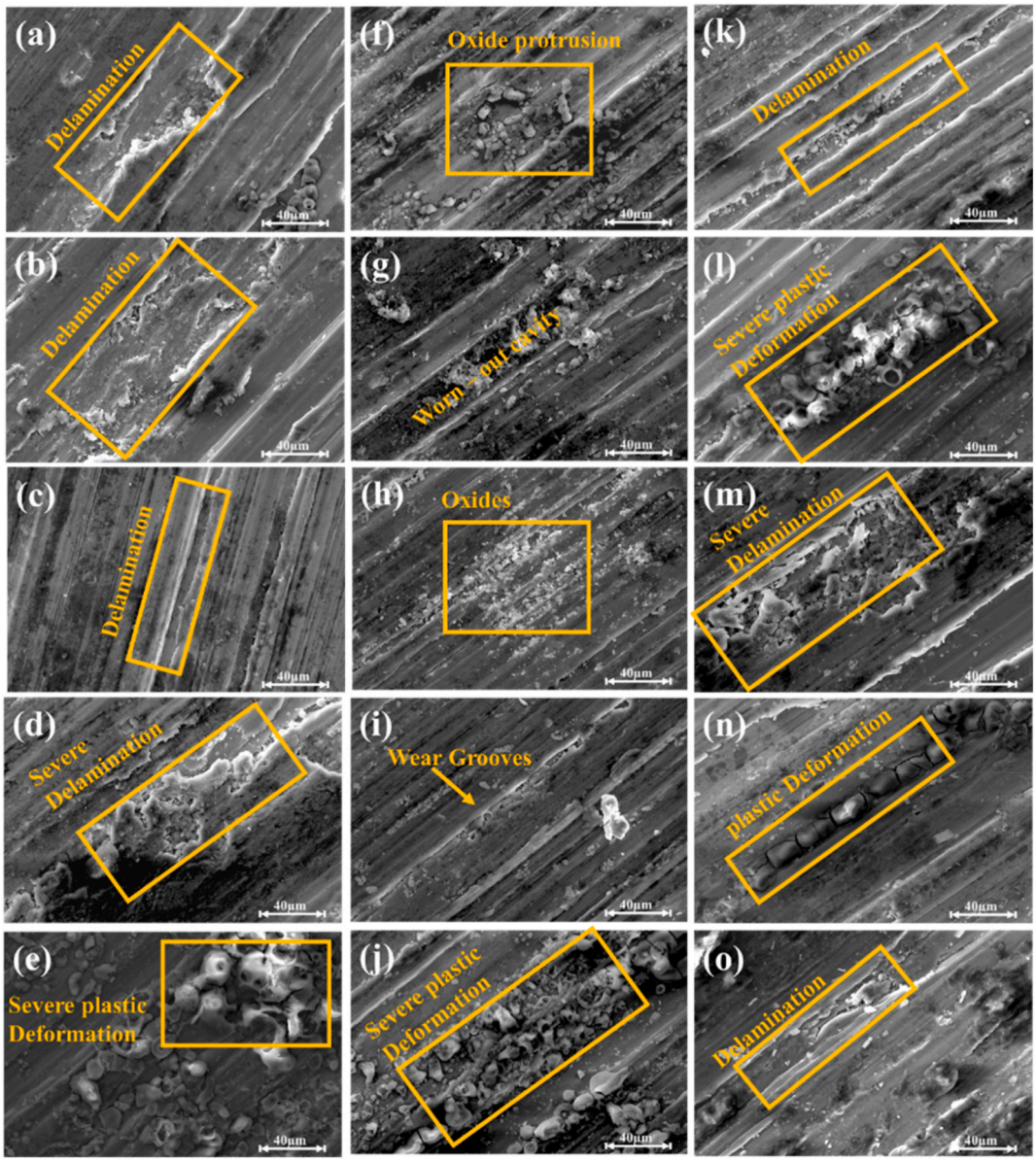

Fig. 6. Wear morphology of (a–e) as-cast; (f–j) T4; (k–o) T6 heat-treated EV31A at wear temperature of (a, f, k) 50 °C; (b, g, l) 100 °C; (c, h, m) 150 °C; (d, i, n) 200 °C; (e, j, o) 250 °C.

rate of 17 mg is observed at 250 °C. Given the strong impact of intermetallic phases, EV31A shows remarkably consistent wear behaviour across the full range of test temperatures. At 150 °C, the alloy's wear rate began to accelerate. The phases present in the T4 heat-treated alloy are identified in Fig. 5(b). In T4 heat-treated alloy at 50 °C, apart from α-Mg, phases such as $Mg_{12}Nd$, Zr-Gd-O, and Zr are observed. After heating, the intermetallic phase dissolved and was not observed in the operating temperature from 100 °C to 250 °C. At 100 °C, along with α-Mg, Gd_2O_3 is observed. In the T4 heat-treated alloy at 150 °C, the wear rate was 20.2 mg, demonstrating that the Mg oxides do not improve the alloy's wear resistance. At wear temperatures between 200 and 250 °C, oxides of magnesium, zirconium, and zinc are visible. The Zr in the alloy is a key factor in its exceptional wear resistance. By examining Fig. 5(c), it is possible to determine the various phases that exist in heat-treated T6 alloy. It reveals that MgO, ZrO_2, and Nd oxides ($Nd_2O_3{\cdot}ZrO_2$) are all present in alloy wear at 50 °C, 100 °C, and 150 °C. It is understood that the wear rate of T6 heat-treated alloy is decreasing to 150 °C; it may be because of the presence of these phases. The Zr_3O phase formed at 200 °C leads to an increase in wear rate to 18.1 mg, and at 250 °C, the presence of Gd_2O_3 and ZrO_2 is observed. Zr and REE (Nd and Gd) oxides are found to be the influencing elements that modify the EV31A alloy's wear behaviour. Gd_2O_3, and Zr_3O, are formed predominantly at a temperature greater than 200 °C. On the other hand, oxides of Nd are identified at the wear samples at 50 °C, 100 °C, and 150 °C. Wear is reduced relative to other test circumstances where Mg and Nd oxides are present, suggesting that these oxides play a substantial role in reducing the alloy's wear rate.

Table 3
Elemental weight percentage of wear EV31A alloy at different operating temperatures.

Condition		Content of elements (wt.%)						
		Mg	Nd	Gd	Zn	Zr	O	Fe
As-Cast	At 50 °C	65.82	2.36	0.86	0.5	0.2	28.61	1.64
	At 100 °C	77.74	2.49	0.95	0.49	0.05	17.86	0.41
	At 150 °C	80.03	2.72	1.02	0.57	0.14	15.28	0.23
	At 200 °C	83.54	2.95	0.90	0.43	–	11.58	0.60
	At 250 °C	82.22	3.34	1.06	0.61	0.16	12.55	–
T4	At 50 °C	69.04	2.78	1.22	0.49	–	26.24	0.23
	At 100 °C	75.45	3.35	1.30	0.63	0.36	18.39	0.52
	At 150 °C	86.10	2.97	1.22	0.52	0.08	8.91	0.20
	At 200 °C	76.64	2.56	0.99	059	0.14	18.50	0.59
	At 250 °C	68.89	2.49	0.84	0.53	0.12	26.94	0.19
T6	At 50 °C	68.62	2.63	1.10	0.41	0.12	26.96	0.17
	At 100 °C	76.05	2.91	1.32	0.53	0.46	18.33	0.39
	At 150 °C	75.38	2.82	1.27	0.46	0.15	18.83	1.09
	At 200 °C	72.70	3.10	0.84	0.51	0.51	22.07	0.26
	At 250 °C	66.74	2.46	0.97	0.45	0.17	28.45	0.76

But the oxides of Gd is not protecting wear. ZrO_2 is protective among Zr oxides, while Zr_3O does not withstand wear. As the oxygen atom per Zr is comparatively high in ZrO_2, where oxygen atom plays a significance role in resisting wear rate. It may be because, the higher hardness of ZrO_2 where hardness is depends on Zr–O bond. Further Zr_3O has hexagonal close pack structure, where ZrO_2 has monoclinic in atmospheric condition and it tends to change into tetragonal and cubic structure upon change in atmospheric conditions [63,64]. Zn does not significantly affect the EV31A wear rate. According to Mg-Nd-Zn phase diagram, Zn has a greater tendency to evaporate or dissipate even at low temperatures when less than 2% weight of it is present along with Nd [64].

3.4. Wear morphology

The wear morphology under each test condition is shown in Fig. 6(a–o). The wear morphology of as-cast EV31A is depicted in Fig. 6 (a–e), where delamination is seen to be the primary wear occurrence at 50 °C, 100 °C, 150 °C, and 200 °C. Notably, severe delamination is observed at 200 °C. At 250 °C, the as-cast alloy undergoes plastic deformation, which may be due to an increase in ductility of the alloy at the expense of hardness. Higher rates of oxide formation in as-cast EV31A can be attributed to the presence of intermetallic phases [32].

When the oxide layer thickness exceeds its critical thickness, it delaminates (peels off or pulls away) from the worn surface [65,66]. This occurs despite the fact that the oxides are produced in the as-cast alloy. Furthermore, the as-cast alloy's intermetallic and REE-rich phases are more brittle and harder than the -Mg phase, which is responsible for abrasive wear. The generation of oxide and moderate delamination influence the wear behaviour of a T4 heat-treated alloy Fig. 5 (f – i). Metal oxides introduce a third body into the wear system, altering the wear rate of the alloy. T4 alloy exhibits considerable plastic deformation at 250 °C, as shown in Fig. 5(j). Localized oxidation is caused by finely scattered precipitates inside grains and along grain borders. T4 heat treatment, on the other hand, dissolves most intermetallic phases, resulting in less oxides being formed in T4 alloy, where the oxide layer thickness may be less critical, limiting delamination [62,67]. Fig. 6 shows that at 250 °C, the T6 heat-treated alloy does not exhibit significant delamination in addition to plastic deformation (k - o). Notably, T6 alloy possesses nearly consistent hardness across all temperature ranges. When a specimen is subjected to high-temperature friction and diffusion, heat is generated, resulting in localized surface melting and, eventually, plastic deformation [62,68]. Also, owing of the tiny grain size and less intermetallic and REE-rich phases, the third body lubricant (oxide layer) phenomena is reduced. The wear morphology supports the existing processes that govern the alloy's wear behaviour. As-cast, T4, and T6 heat-treated EV31A alloys exhibit delamination, oxide formation, and delamination owing to plastic deformation. The alloy, with the exception of T6 heat-treated alloy, experiences severe plastic deformation at 250 °C. Delamination, oxidation, and plastic deformation are all features of abrasive, corrosive, and adhesive wear.

After a dry sliding wear test, Table 3 reveals the elemental mapping of the test specimens. Oxygen content in as-cast EV31A is found to decrease with increasing wear temperature. Mild wear conditions are represented by the production of oxides. This indicates that as-cast EV31A undergoes a change from mild wear to severe wear as temperatures rise. The opposite is true for heat-treated (T4 and T6) EV31A, where oxygen percentage drops up to 150 °C and subsequently increases with further temperature increases. This finding suggests that the wear behaviour of T4 and T6 heat-treated alloys are comparable. The material transfer from counterpart to pin (EV31A) is confirmed by the presence of Iron (Fe) on the test specimen as represented in Table 3. During plastic deformation, the material transfer from counterpart to test specimen is very less (negligible).

Fig. 7 (a – o) shows the wear debris of the test specimens under all test conditions, and it helps to ensure the previously discussed wear mechanism. Figure (a–e) shows the wear debris of as-cast EV31A, where the delaminated debris in the form of a long string-like structure is observed at 50 °C, 100 °C, and 150 °C as shown in Fig. 7 (a – c), which confirms the delamination of the EV31A at the operating temperature. Along with delamination, the formation of the oxides is observed at 50 °C, 100 °C, and 150 °C. The severe delaminated debris is noted in Fig. 7 (d). Fig. 7 (e) evidenced that the incipient melting resulted in plastic deformation of the EV31A alloy. In the case of as-cast alloy, an increase in operating temperature leads to an increase in brittleness of the alloy up to 200 °C and

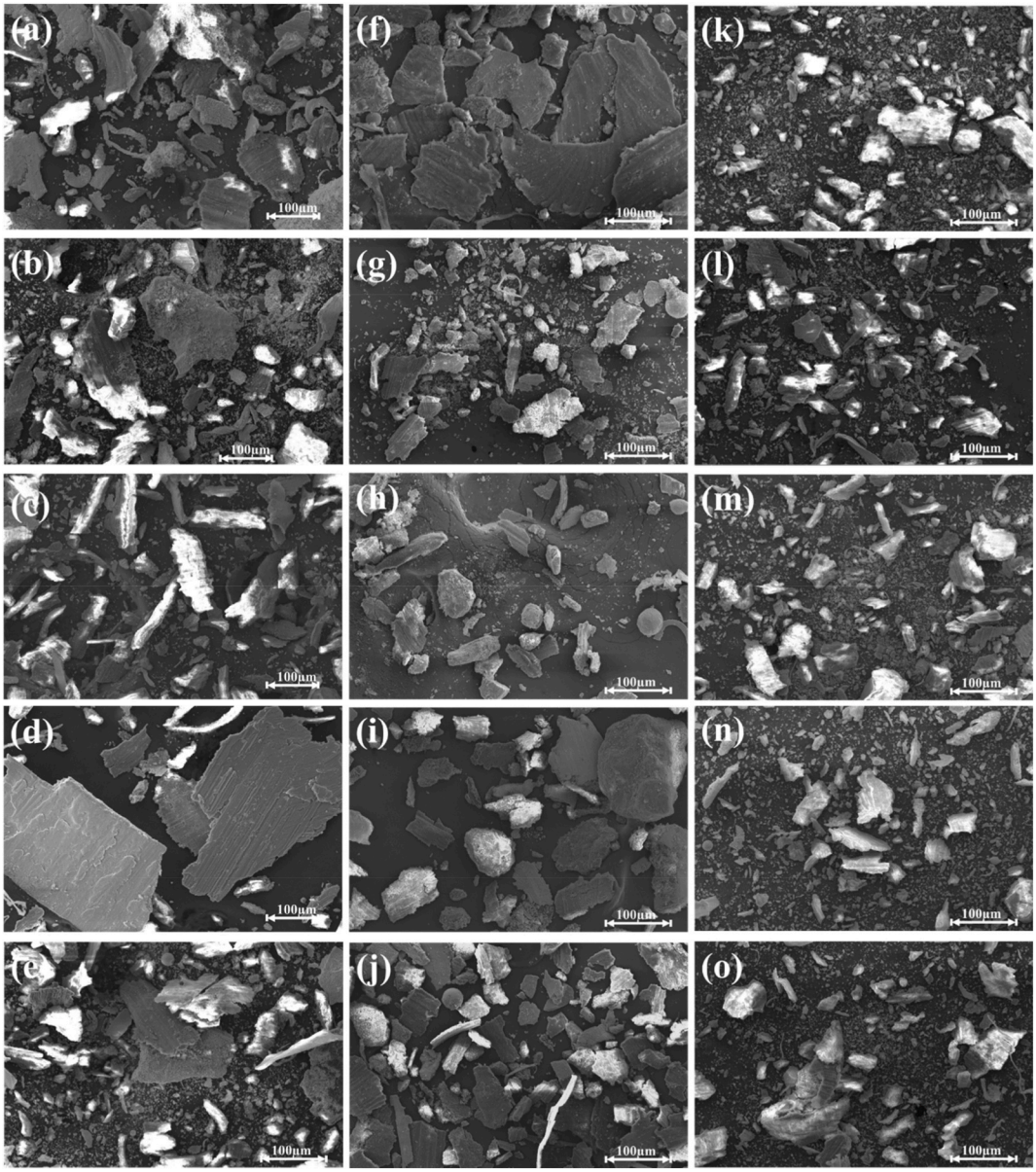

Fig. 7. Secondary electron image of wear debris of EV31A at all test conditions (a–e) as-cast; (f–j) T4; (k–o) T6 heat-treated EV31A at wear temperature of (a, f, k) 50 °C; (b, g, l) 100 °C; (c, h, m) 150 °C; (d, i, n) 200 °C; (e, j, o) 250 °C.

then the alloy shows plastic deformation due to melting. Fig. 7 (f – j) and (k – o) show the T4 and T6 EV31A debris, respectively. It is noted that the debris of nearly similar size in T4 and T6 heat-treated alloy. Further, the round edge debris corresponds to plastically deformed EV31A, and debris with a sharp edge represents the delamination observed in Fig. 7 (j) and (o).

Table 4 shows the elemental weight percentage of wear debris of as-cast, T4, and T6 EV31A under test conditions. Compared to Mg, the oxygen content is higher in all test conditions, implying the oxidation of Mg at elevated temperature wear test. Also, the oxygen content is nearly the same in the debris of all operating temperatures. The presence of oxygen also confirmed the involvement of third body lubricant (metal oxides) in the wear behaviour of EV31A. The Fe content on the debris decreases with heat treatment, which may be because of the phase changes happens in EV31A.

3.5. Prediction of tribological properties by machine learning approach

The importance of process parameters concerning response variables is estimated using F-test as shown in Fig. 8 (a – b). It shows that the temperature greatly influences the CoF of EV31A as it alters the solubility of elements and phases present in it. On other hand, applied normal load strongly influences the wear rate of the alloy. Also, temperature increases lead to severe plastic deformation as a

Table 4
Elemental weight percentage of wear debris as-cast EV31A alloy at different operating temperatures.

Condition		Content of elements (wt.%)						
		Mg	Nd	Gd	Zn	Zr	O	Fe
As-Cast	50 °C	34.2	0.5	–	–	0.1	42.3	22.9
	100 °C	34.2	0.5	–	–	0.1	42.3	22.9
	150 °C	35.0	0.3	0.3	0.2	0.3	49.3	14.6
	200 °C	33.8	0.2	–	0.6	–	50.5	14.8
	250 °C	11.0	–	–	2.6	–	72.3	14.2
T4	50 °C	45.9	–	–	0.4	–	44.9	8.8
	100 °C	42.6	0.6	0.1	0.3	0.4	52.5	3.5
	150 °C	41.6	–	0.8	0.1	0.6	48.5	8.4
	200 °C	38.0	0.1	0.4	0.3	0.7	58.1	2.4
	250 °C	39.5	0.4	0.3	0.1	0.1	52.0	7.5
T6	50 °C	43.1	1.1	0.6	0.3	0.2	50.4	4.3
	100 °C	40.0	1.1	0.4	0.5	0.2	53.4	4.4
	150 °C	40.4	1.3	0.7	0.3	0.1	55.1	2.1
	200 °C	46.1	1.5	0.6	0.2	0.3	49.5	1.8
	250 °C	44.2	1.4	0.5	0.4	–	51.4	2.1

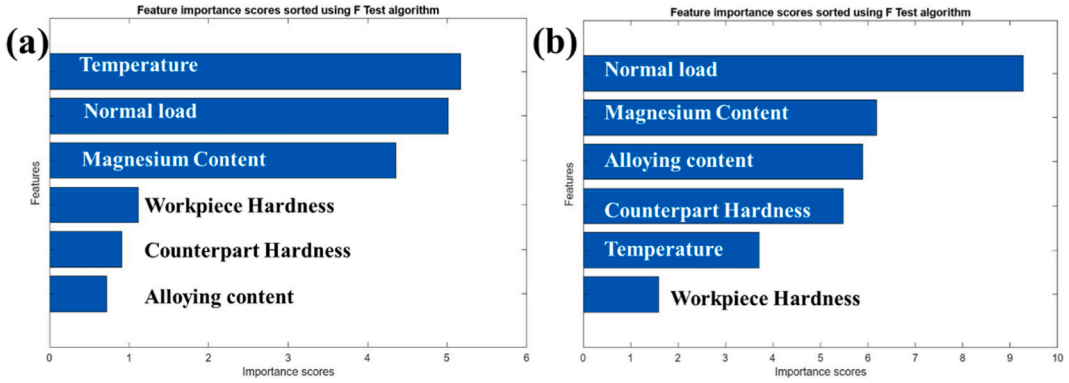

Fig. 8. Importance of process parameters sorted using F test for (a) CoF; (b) Wear rate.

result of an increase in the ductility of the material. In general, the increase in temperature leads to a decrease in CoF, but the hardness which increases with the heat treatment process and varies with operating temperature has a significant influence on the response. Fig. 8 (b), confirms normal load and magnesium content have significant influence on wear rate, but these parameters are constant in the study. Hence the wear rate achieved during the experimentation are nearly linear as shown in Fig. 9 (b). It also illustrates that the importance of operating temperature (very less) on wear rate of the EV31A.

The ability of ML modelling (SVM and ANN) to predict tribological properties of EV31A with the predefined dataset is demonstrated in Fig. 9 (a – b). The quality of the ML modelling is defined by the performance parameters as shown in Table 5. By comparing all performance parameters ANN model shows good correlation with experimental results with R^2 of 0.99 and 0.89 in predicting CoF, and wear rate, respectively. Especially, the fine Gaussian SVM model shows the RMSE value of CoF and wears rate as 0.067589, and 0.001412; Trilayered ANN shows the RMSE of CoF and wear rate as 0.018064, and 0.000992, respectively. It is recognized that ANN better model to predict tribological parameters with the limited dataset [29]. Further it is also found that SVM model required large dataset to predict the response with greater accuracy, working in SVM with small number of data leads to unreliable results. When comparing the predicted value of CoF and wear rate, ANN-predicted CoF shows a good correlation with experimental CoF; even though SVM-predicted wear rate shows a good R^2, and RMSE value, it is not fitted/correlated with the experimental wear rate as shown in Fig. 9(b). Further, the ANN-predicted wear rate follows the nearly same trend as experimental data. This is because the normal load is the high influencing parameter for wear rate which is constant in the experimentation of the study.

4. Conclusion

The study evaluated the high-temperature dry sliding wear behaviour of EV31A Mg alloy in both quantitative as well as qualitative aspects. The wear coefficient (K) is greater than 10^{-4} in all test conditions, which implies that severe wear happens at the operating temperature range of 50 °C – 250 °C with a normal load of 10 N and sliding distance of 1000 m. By comparing CoF and wear rate of as-cast, T4, and T6 EV31A alloy, the as-cast alloy shows optimal wear rate with comparatively high CoF. It is advised to use EV31A alloy in its as-cast form for applications where a low wear rate is desired at the expense of mechanical properties. The oxides of Mg and Gd are not restricting the wear, but it is restricted by the oxides of Nd and Zr. The Zn does not show a significant influence on the wear

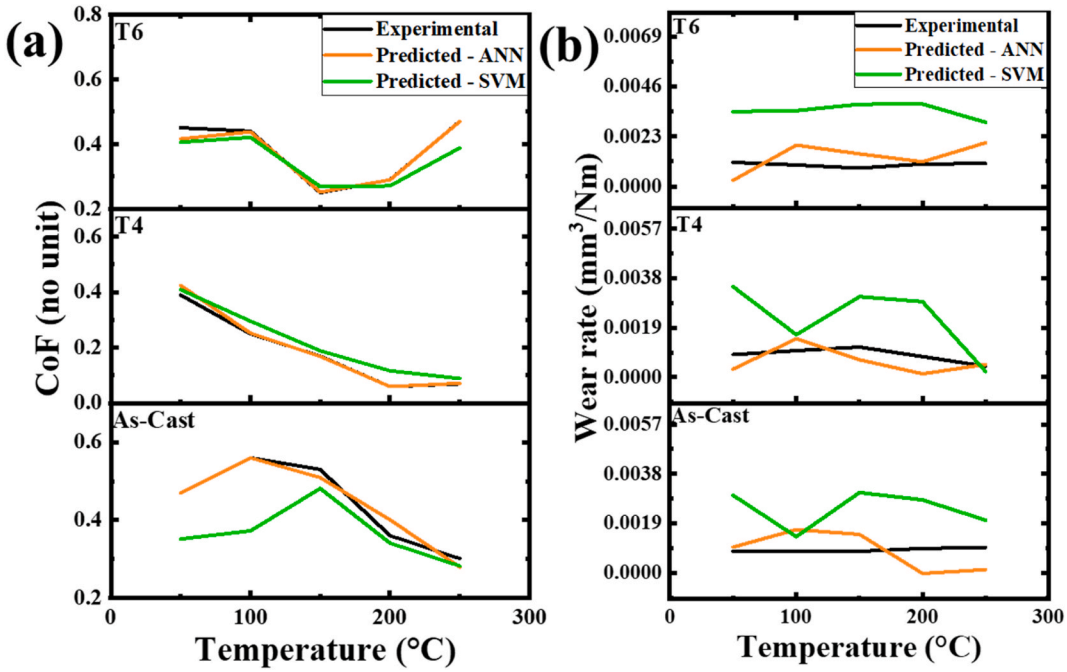

Fig. 9. Comparison of predicted vs experimental (a) CoF; (b) Wear rate.

Table 5
Performance metrics of predicted tribological parameters

ML models	R^2	RMSE	MSE	MAE
CoF - SVM	0.80	0.067589	0.004568	0.049097
CoF - ANN	0.99	0.018064	0.000326	0.010783
Wear - SVM	0.77	0.001412	1.9×10^{-6}	0.001132
Wear - ANN	0.89	0.000992	9.8×10^{-7}	0.000832

behaviour of EV31A. Delamination, oxide formation, and delamination along with plastic deformation, respectively, occur in the EV31A alloy in its as-cast, T4, and T6 states. The ANN model is identified as a promising method to predict tribological properties with a limited dataset. It shows a maximum R^2 of 0.99 and 0.89 in ANN prediction of CoF and wear rate, respectively. Even though the normal load is constant in the study, the machine learning approach defines the operating temperature and average load are the most influencing parameter in CoF, and wear rate, respectively.

Author contribution statement

Somasundaram M: Performed the experiments; Analyzed and interpreted the data; Wrote the paper.
U. NarendraKumar; A. Muthuchamy: Analyzed and interpreted the data; Wrote the paper.
A. Raja Annamalai: Conceived and designed the experiments; Analyzed and interpreted the data; Contributed reagents, materials, analysis tools or data; Wrote the paper.

Data availability statement

Data will be made available on request.

Declaration of competing interest

The authors declare that they have no known competing financial interests or personal relationships that could have appeared to influence the work reported in this paper.

References

[1] V.A. Yartys, et al., Magnesium based materials for hydrogen based energy storage: past, present and future, Int. J. Hydrogen Energy 44 (15) (Mar. 2019) 7809–7859, https://doi.org/10.1016/j.ijhydene.2018.12.212.

[2] M.K. Kulekci, Magnesium and its alloys applications in automotive industry, Int. J. Adv. Manuf. Technol. 39 (9–10) (Nov. 2008) 851–865, https://doi.org/10.1007/s00170-007-1279-2.

[3] S.V.S. Prasad, S.B. Prasad, K. Verma, R.K. Mishra, V. Kumar, S. Singh, The role and significance of Magnesium in modern day research-A review, J. Magnesium Alloys 10 (1) (Jan. 2022) 1–61, https://doi.org/10.1016/j.jma.2021.05.012.

[4] F. Czerwinski, Controlling the ignition and flammability of magnesium for aerospace applications, Corrosion Sci. 86 (Sep. 2014) 1–16, https://doi.org/10.1016/j.corsci.2014.04.047.

[5] F. Czerwinski, The reactive element effect on high-temperature oxidation of magnesium, Int. Mater. Rev. 60 (5) (Jun. 2015) 264–296, https://doi.org/10.1179/1743280415Y.0000000001.

[6] F. Czerwinski, Factors affecting the oxidation nature of magnesium alloys, JOM 56 (5) (May 2004) 29–31, https://doi.org/10.1007/s11837-004-0123-5.

[7] D.J. Lloyd, Particle reinforced aluminium and magnesium matrix composites, Int. Mater. Rev. 39 (1) (Jan. 1994) 1–23, https://doi.org/10.1179/imr.1994.39.1.1.

[8] M. Gupta, N.M.L. Sharon, Magnesium, magnesium alloys, and magnesium composites, in: Magnesium, Magnesium Alloys, and Magnesium Composites, John Wiley & Sons, Inc., Hoboken, NJ, USA, 2010, https://doi.org/10.1002/9780470905098.fmatter.

[9] K. Ponappa, S. Aravindan, P.V. Rao, Influence of Y_2O_3 particles on mechanical properties of magnesium and magnesium alloy (AZ91D), J. Compos. Mater. 47 (10) (May 2013) 1231–1239, https://doi.org/10.1177/0021998312446501.

[10] D. Eliezer, E. Aghion, F.H. (Sam) Froes, Magnesium science, technology and applications, Adv. Perform. Mater. 5 (3) (Dec. 1998) 201–212, https://doi.org/10.1023/A:1008682415141.

[11] S.N. Mathaudhu, E.A. Nyberg, Magnesium alloys in U.S. Military applications: past, current and future solutions, Magnes. Technol. 6 (2010).

[12] G. Wu, C. Wang, M. Sun, W. Ding, Recent developments and applications on high-performance cast magnesium rare-earth alloys, J. Magnesium Alloys 9 (1) (Jan. 2021) 1–20, https://doi.org/10.1016/j.jma.2020.06.021.

[13] L. Ren, et al., Magnesium application in railway rolling stocks: a new challenge and opportunity for lightweighting, Int. J. Lightweight Mater. Manuf. 1 (2) (Jun. 2018) 81–88, https://doi.org/10.1016/j.ijlmm.2018.05.002.

[14] J. Chai, Y. Zhou, X. Zhou, S. Wang, Z.G. Zhang, Z. Liu, Analysis on shock effect of China's high-speed railway on aviation transport, Transp. Res. Part Policy Pract. 108 (Feb. 2018) 35–44, https://doi.org/10.1016/j.tra.2017.12.001.

[15] Jeong Gil Cho, Jeong Seo Koo, Hyun Seung Jung, A lightweight design approach for an EMU carbody using a material selection method and size optimization, J. Mech. Sci. Technol. 30 (2016) 673–681, https://doi.org/10.1007/s12206-016-0123-8.

[16] M.S. Pereira, J.a.C. Ambrósio, J.P. Dias, Crashworthiness analysis and design using rigid–flexible multibody dynamics with application to train vehicles, Int. J. Numer. Methods Eng. 40 (4) (1997) 655–687, https://doi.org/10.1002/(SICI)1097-0207(19970228)40:4<655::AID-NME84>3.0.CO;2-N.

[17] P.J. Hodgson, D. Forsey, THE DESIGN OF LIGHTWEIGHT INTER-CITY COACH STRUCTURES, Railw. Veh. BODY Struct., 1985. Dec. 05, 2022. [Online]. Available: https://trid.trb.org/view/231813.

[18] Q. Yang, A.K. Ghosh, Deformation behavior of ultrafine-grain (UFG) AZ31B Mg alloy at room temperature, Acta Mater. 54 (19) (Nov. 2006) 5159–5170, https://doi.org/10.1016/j.actamat.2006.06.043.

[19] L.M. Calado, M.J. Carmezim, M.F. Montemor, Rare earth based magnesium alloys—a review on WE series, Front. Mater. 8 (Jan. 2022), 804906, https://doi.org/10.3389/fmats.2021.804906.

[20] S.K. Sharma, et al., Significance of alloying elements on the mechanical characteristics of Mg-based materials for biomedical applications, Crystals 12 (8) (Aug. 2022) 1138, https://doi.org/10.3390/cryst12081138.

[21] P. Poddar, A. Das, K.L. Sahoo, Dry sliding wear characteristics of gravity die-cast magnesium alloys, Metall. Mater. Trans. A 45 (4) (2013) 2270.

[22] K.K. Ajith Kumar, U.T.S. Pillai, B.C. Pai, M. Chakraborty, Dry sliding wear behaviour of Mg–Si alloys, Wear 303 (1) (Jun. 2013) 56–64, https://doi.org/10.1016/j.wear.2013.02.020.

[23] J. Zhang, A.T. Alpas, Transition between mild and severe wear in aluminium alloys, Acta Mater. 45 (2) (Feb. 1997) 513–528, https://doi.org/10.1016/S1359-6454(96)00191-7.

[24] C. Taltavull, B. Torres, A.J. López, J. Rams, Dry sliding wear behavior of AM60B magnesium alloy, Wear 301 (1) (Apr. 2013) 615–625, https://doi.org/10.1016/j.wear.2012.11.039.

[25] C. Taltavull, P. Rodrigo, B. Torres, A.J. López, J. Rams, Dry sliding wear behavior of AM50B magnesium alloy, Mater. Des. 56 (Apr. 2014) 549–556, https://doi.org/10.1016/j.matdes.2013.12.015, 1980-2015.

[26] H. Chen, A.T. Alpas, Sliding wear map for the magnesium alloy Mg-9Al-0.9 Zn (AZ91), Wear 246 (1) (Nov. 2000) 106–116, https://doi.org/10.1016/S0043-1648(00)00495-6.

[27] J. An, W. Zhao, C.Q. Feng, Elevated-temperature wear characteristics and mild-severe wear transition in the Mg–10.1Gd–1.4Y–0.4Zr alloy, J. Tribol. 141 (12) (Dec. 2019), 121601, https://doi.org/10.1115/1.4044654.

[28] M.B. Gorji, A. de Pannemaecker, S. Spevack, Machine learning predicts fretting and fatigue key mechanical properties, Int. J. Mech. Sci. 215 (Feb. 2022), 106949, https://doi.org/10.1016/j.ijmecsci.2021.106949.

[29] S. Baydoun, M. Fartas, S. Fouvry, Comparison between physical and machine learning modeling to predict fretting wear volume, Tribol. Int. 177 (Jan. 2023), 107936, https://doi.org/10.1016/j.triboint.2022.107936.

[30] F. Aydin, R. Durgut, M. Mustu, B. Demir, Prediction of wear performance of ZK60/CeO2 composites using machine learning models, Tribol. Int. 177 (Jan. 2023), 107945, https://doi.org/10.1016/j.triboint.2022.107945.

[31] S.G. Mukunda, A. Srivastava, S.B. Boppana, S. Dayanand, D. Yeshwanth, Wear performance prediction of MWCNT-reinforced AZ31 composite using machine learning technique, J. Bio- Tribo-Corros. 9 (2) (Jun. 2023) 1–13, https://doi.org/10.1007/s40735-023-00745-w.

[32] M. Somasundaram, U. NarendraKumar, Electrochemical corrosion behaviour of stir cast and heat-treated EV31A magnesium alloy in different electrolytic mediums, J. Appl. Electrochem. (2022), https://doi.org/10.1007/s10800-022-01778-8.

[33] M. Somasundaram, U. NarendraKumar, A.R. Annamalai, The oxidation behavior of stir-cast and heat-treated EV31A at high temperatures in an air atmosphere, Corrosion Sci. 211 (Feb. 2023), 110894, https://doi.org/10.1016/j.corsci.2022.110894.

[34] M. Somasundaram, U. NarendraKumar, Microstructural and mechanical properties of a heat-treated EV31A magnesium alloy fabricated using the stir-casting process, Crystals 12 (8) (Aug. 2022) 1163, https://doi.org/10.3390/cryst12081163.

[35] Y. Wang, C. Wu, L. Zhang, P. Qu, S. Li, Z. Jiang, Thermal oxidation and its effect on the wear of Mg alloy AZ31B, Wear 476 (Jul. 2021), 203673, https://doi.org/10.1016/j.wear.2021.203673.

[36] K. Takagi, E. Hashamova, M. Dienwiebel, Y. Mine, K. Takashima, Correlation of wear behaviour and microstructural evolution in Mg–Zn–Y alloys with long-period stacking ordered phase, Wear 482–483 (Oct. 2021), 203983, https://doi.org/10.1016/j.wear.2021.203983.

[37] A. Prasad, J. Jain, N.N. Gosvami, Effect of minor La addition on wear behaviour of Mg-10Dy alloy, Wear 486–487 (Dec. 2021), 204121, https://doi.org/10.1016/j.wear.2021.204121.

[38] M. Venkataiah, T. Anup Kumar, K. Venkata Rao, S. Anand Kumar, R. Dumpala, B. Ratna Sunil, Investigation on the role of microstructure and temperature on tribological characteristics of fine-grained ZE41 Mg alloy, Tribol. Mater. Surface Interfac. 16 (1) (Jan. 2022) 68–75, https://doi.org/10.1080/17515831.2021.1951539.

[39] T. Li, X.-T. Wang, S.-Q. Tang, Y.-S. Yang, J.-H. Wu, J.-X. Zhou, Improved wear resistance of biodegradable Mg–1.5Zn–0.6Zr alloy by Sc addition, Rare Met. 40 (8) (Aug. 2021) 2206–2212, https://doi.org/10.1007/s12598-020-01420-6.

[40] J.R. Deepak, N. Joy, T. Arunkumar, R. Srivatsan, R. Gnanasekar, Tribological investigation of magnesium rare earth alloy for orthopedic application, Mater. Today Proc. 47 (2021) 4767–4771, https://doi.org/10.1016/j.matpr.2021.05.675.
[41] Q. Chen, Y. Yu, J. Sun, C. Jing, Y. Zhao, J. Wang, Investigation of the wear behavior of surface welding AZ91 and AZ91+Gd alloys under variable loading conditions, Crystals 11 (5) (May 2021) 554, https://doi.org/10.3390/cryst11050554.
[42] L. Tonelli, L. Pezzato, P. Dolcet, M. Dabalà, C. Martini, Effects of graphite nano-particle additions on dry sliding behaviour of plasma-electrolytic-oxidation-treated EV31A magnesium alloy against steel in air, Wear 404 (405) (Jun. 2018) 122–132, https://doi.org/10.1016/j.wear.2018.03.012.
[43] A. Zafari, H.M. Ghasemi, R. Mahmudi, Effect of rare earth elements addition on the tribological behavior of AZ91D magnesium alloy at elevated temperatures, Wear 303 (1–2) (Jun. 2013) 98–108, https://doi.org/10.1016/j.wear.2013.02.016.
[44] M. Nouri, X. Sun, D.Y. Li, Beneficial effects of yttrium on the performance of Mg–3%Al alloy during wear, corrosion and corrosive wear, Tribol. Int. 67 (Nov. 2013) 154–163, https://doi.org/10.1016/j.triboint.2013.07.012.
[45] A.J. Smola, B. Schölkopf, A tutorial on support vector regression, Stat. Comput. 14 (3) (Aug. 2004) 199–222, https://doi.org/10.1023/B:STCO.0000035301.49549.88.
[46] A. Elen, S. Baş, C. Közkurt, An adaptive Gaussian kernel for support vector machine, Arabian J. Sci. Eng. 47 (8) (Aug. 2022) 10579–10588, https://doi.org/10.1007/s13369-022-06654-3.
[47] D.K. Jana, P. Bhunia, S.D. Adhikary, A. Mishra, Analyzing of salient features and classification of wine type based on quality through various neural network and support vector machine classifiers, Results Control Optim 11 (Jun. 2023), 100219, https://doi.org/10.1016/j.rico.2023.100219.
[48] G. Brassington, Mean Absolute Error and Root Mean Square Error: Which Is the Better Metric for Assessing Model Performance? Apr, 2017, p. 3574.
[49] A.F. Siegel, Chapter 15 - anova: testing for differences among many samples and much more, in: A.F. Siegel (Ed.), Practical Business Statistics, seventh ed., Academic Press, 2016, pp. 469–492, https://doi.org/10.1016/B978-0-12-804250-2.00015-8.
[50] E04 Committee, Test Methods for Determining Average Grain Size, ASTM International, 2021, https://doi.org/10.1520/E0112-13R21.
[51] W.D. Callister, D.G. Rethwisch, Materials Science and Engineering: an Introduction, vol. 7, John wiley & sons, New York, 2007.
[52] J.-F. Nie, Precipitation and hardening in magnesium alloys, Metall. Mater. Trans. A 43 (11) (Nov. 2012) 3891–3939, https://doi.org/10.1007/s11661-012-1217-2.
[53] A. Nayeb-Hashemi, Phase diagrams of binary magnesium alloys, ASM Int. Met. Park Ohio 44073 USA 370 (1988) 1988.
[54] B. Smola, I. Stulıková, F. Von Buch, B.L. Mordike, Structural aspects of high performance Mg alloys design, Mater. Sci. Eng. A 324 (1–2) (2002) 113–117.
[55] T.A. Freeney, R.S. Mishra, Effect of friction stir processing on microstructure and mechanical properties of a cast-magnesium–rare earth alloy, Metall. Mater. Trans. A 41 (2010) 73–84.
[56] D.H. StJohn, M.A. Qian, M.A. Easton, P. Cao, Z. Hildebrand, Grain refinement of magnesium alloys, Metall. Mater. Trans. A 36 (7) (2005) 1669–1679.
[57] C. Tian, X. Li, H. Li, G. Guo, L. Wang, Y. Rong, The effect of porosity on the mechanical property of metal-bonded diamond grinding wheel fabricated by selective laser melting (SLM), Mater. Sci. Eng. A 743 (Jan. 2019) 697–706, https://doi.org/10.1016/j.msea.2018.11.138.
[58] S.-J. Huang, A. Abbas, Effects of tungsten disulfide on microstructure and mechanical properties of AZ91 magnesium alloy manufactured by stir casting, J. Alloys Compd. 817 (Mar. 2020), 153321, https://doi.org/10.1016/j.jallcom.2019.153321.
[59] A. Jana, M. Das, V.K. Balla, Effect of heat treatment on microstructure, mechanical, corrosion and biocompatibility of Mg-Zn-Zr-Gd-Nd alloy, J. Alloys Compd. 821 (Apr. 2020), 153462, https://doi.org/10.1016/j.jallcom.2019.153462.
[60] Glossary of Terms and Definitions in the Field of Friction, Wear and Lubrication; Tribology, Organisation for Economic Co-operation and Development, Paris, 1969.
[61] J.F. Archard, Contact and rubbing of flat surfaces, J. Appl. Phys. 24 (8) (Aug. 1953) 981–988, https://doi.org/10.1063/1.1721448.
[62] S.k. Biswas, Wear of metals, in: Wear – Materials, Mechanisms and Practice, John Wiley & Sons, Ltd, 2005, pp. 21–36, https://doi.org/10.1002/9780470017029.ch3.
[63] J. Zhang, A.R. Oganov, X. Li, H. Dong, Q. Zeng, Novel compounds in the Zr–O system, their crystal structures and mechanical properties, Phys. Chem. Chem. Phys. 17 (26) (2015) 17301–17310, https://doi.org/10.1039/C5CP02252E.
[64] L.L. Rokhlin, Magnesium alloys containing rare earth metals: structure and properties, in: Advances in Metallic Alloys vol. 3, Taylor & Francis, London ; New York, 2003.
[65] P. Lacombe, Physical Chemistry of the Solid State: Applications to Metals and Their Compounds, Sep. 1983, pp. 19–23.
[66] G.W. Stachowiak, A.W. Batchelor, Engineering Tribology, Butterworth-Heinemann, 2013.
[67] T.F.J. Quinn, The effect of 'hot-spot' temperatures on the unlubricated wear of steel, OR Trans. 10 (2) (Jan. 1967) 158–168, https://doi.org/10.1080/05698196708972175.
[68] K.-H.Z. Gahr, Microstructure and Wear of Materials, Elsevier, 1987.